ACS OMEGA

http://pubs.acs.org/journal/acsodf

Article

Cu-BDC and Cu_2O Derived from Cu-BDC for the Removal and Oxidation of Asphaltenes: A Comparative Study

Abhishek Nayak, Shanon Viegas, Harshini Dasari, and Nethaji Sundarabal*

Cite This: *ACS Omega* 2022, 7, 34966−34973

Read Online

ACCESS | Metrics & More | Article Recommendations | Supporting Information

ABSTRACT: Asphaltenes have been associated with a number of problems in the petroleum industry with regard to the storage, exploration, and transportation of petroleum crude. In the current work, Copper-BenzeneDiCarboxylic acid (Cu-BDC) and Cu-BDC derived metal oxide has been used in the removal and oxidation of the asphaltenes. The MOF derived metal oxide was confirmed to be Cu_2O. Though adsorption of asphaltenes followed a Langmuir adsorption isotherm in both cases, Cu-BDC was superior to Cu_2O with an adsorption capacity four times that of the adsorption capacity of Cu_2O. Also, the kinetic studies showed that the adsorption kinetics followed pseudo second order adsorption kinetics in both cases. From the oxidation studies, it was found that Cu-BDC was unstable beyond 350 °C and had no role in catalyzing the oxidation reaction. The Cu_2O, however, was successful at catalyzing the asphaltene oxidation reaction and a reduction of 50 °C in oxidation temperature was observed. Hence comparing Cu-BDC with Cu_2O, MOF was successful in the adsorption reaction but the MOF derived metal oxide had the upper hand in the oxidation reaction.

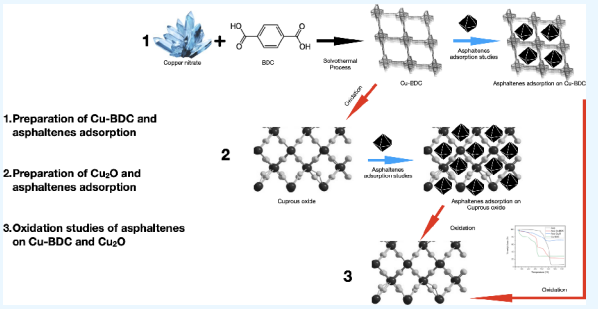

INTRODUCTION

In recent years, the demand for fossil fuels has become challenging due to supply issues because of the near exhaustion of the light crude. The time is nigh for the exploration of heavy crude to meet the current energy needs. The production, transportation, and refining of heavy crude are always associated with the problems of asphaltenes.[1] Asphaltenes are the most polar class of compounds in crude. They are insoluble in paraffinic solvents like *n*-heptane, *n*-hexane, and *n*-pentane while being soluble in aromatic solvents like benzene and toluene. The properties of the asphaltenes have been known to be specific to the geographic location of the crude well. The asphaltenes have been studied for decades and only polarity and basic composition (aromatic compounds, heterocyclic compounds, branched chain) have been found to be similar for different crudes. Due to the complications of the asphaltenes, the heavy crude was often side-lined and as much as 70−80% of the original oil in place is not recovered due to economics.[2] The problems are caused because of the inherent property of asphaltenes to self-aggregate.[3] Asphaltenes in the reservoir exist in the form of nano aggregates but as the production progresses, due to the concentration, temperature, and pressure changes, it loses stability and forms clusters to precipitate in the pores of reservoir rocks and the production lines to reduce the production drastically. The asphaltenes are found to precipitate in the transport line thereby posing problems in transportation.[4] In addition, with as little as 20% asphaltenes in the crude, the viscosity increases by roughly 350 times.[5] During refining, asphaltenes have been reported to clog various units such as heat exchangers, pipelines, and the pores of the catalysts in hydrotreating.

The asphaltenes problem has been serious in petroleum industries but very few strategies are pursued to tackle the precipitation problem. Recently, various methods have been studied to overcome the problem, among which the prediction model of asphaltene precipitation and adsorption by nanoparticles are noteworthy. The asphaltene precipitation prediction model revolves around the control of parameters such as temperature and pressure. The adsorption method has been tested around the world in various laboratories, with various materials. The adsorption process is followed by the oxidation of asphaltenes on the adsorbent for regeneration of the adsorbent. Regeneration is an energy intensive process and requires high temperature heating to the range of 530 °C. Hence, an ideal adsorbent also takes part in the oxidation process in addition to the adsorption. Predominantly, d-block metal oxide nanoparticles, such as Fe_3O_4,[6] are used in the adsorption of asphaltenes for its affinity toward various functional groups of asphaltenes.[7] In addition to d block, recent investigations were carried out using S block and P

Received: June 8, 2022
Accepted: August 8, 2022
Published: September 20, 2022

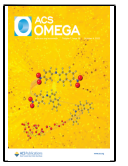

https://doi.org/10.1021/acsomega.2c03574
ACS Omega 2022, 7, 34966−34973

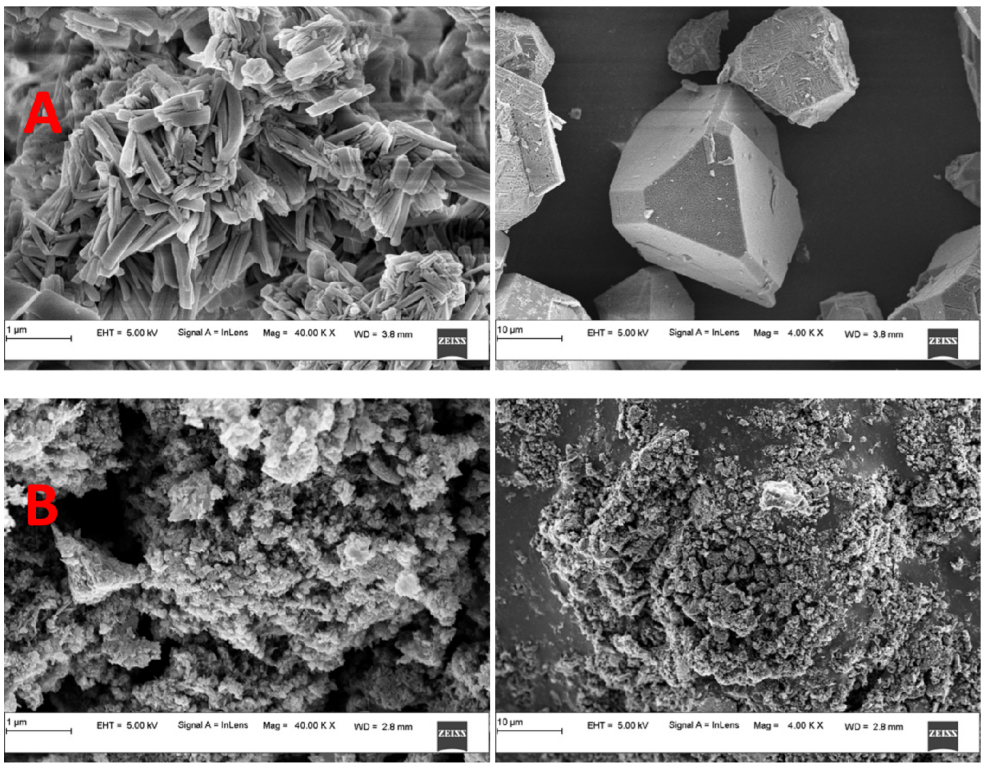

Figure 1. FESEM micrographs of (A) Cu-BDC and (B) Cu_2O.

block oxides such as MgO, CaO, SiO_2, and Al_2O_3 nanoparticles.[8] Various natural minerals like dolomite, calcite, kaolin,[9] and industrial adsorbents like NiO[10] and Aerosil[11] had been studied. Recently, studies involving functionalized nanoparticles (Si and gold functionalized using thiol)[12] and carbon based materials like carbon nanotubes[13] had reported better results.

Although there had been studies on metal oxides for adsorption of asphaltenes, very few published works could be found on metal organic frameworks (MOFs). MOFs are well-known in the field of adsorption because of their high surface area and tunable properties.[14] MOFs have been explored in the areas of gas storage, gas separation, and adsorption owing to the surface properties. Some of the applications involve the gas separation and storage materials for CO_2,[15] H_2S,[16] SO_2,[17] H_2,[18] CH_4,[19] and many more. In addition to the separation of the gases, the MOFs have also been used as sensor materials for dye sensing and the adsorption[20] of heavy metals such as Pb[21] and Cr[22] from water. Hence, a wide range of applications of MOFs in the field of adsorption can be identified. MOFs have been proven to be a good adsorbent for the adsorption of an ionic compound. Despite their proven adsorption properties, MOFs have not been explored for the adsorption of asphaltenes. Even though the MOFs are attractive in adsorption, they fail at high-temperature reactions,[23] thereby restricting its use in adsorption and low temperature reactions. Typically, metal oxides and other classes of materials are preferred over MOFs because the organic linkers forming the framework do not withstand high temperatures. Inherently, most of the MOFs undergo organic decomposition at temperatures ranging from 250 °C to 400 °C, whereas the asphaltenes oxidize around 530 °C. Hence, the application of MOFs for the adsorption and oxidation of asphaltenes have not been explored. In this work, unlike the traditional way of using MOFs as the adsorbent, an attempt is made to compare the adsorptive and oxidative properties of MOFs and its derived metal oxide. The study also promotes the use of MOF derived metal oxide as a reuse strategy for MOFs diverting from the one time use strategy, thereby providing a practical and economic strategy.

RESULTS AND DISCUSSION

Characterization of Prepared Cu-BDC and Metal Oxide Derived from Cu-BDC. The prepared Cu-BDC and Cu derived Cu_2O was characterized using XRD, FTIR, FESEM, BET, and EDAX. From Figure 1, the FESEM obtained for Cu-BDC had a rod-like surface morphology at 1 μm magnification. The material was arranged in an irregular manner with randomly oriented rods. The radius of the rods was found to be around 200 nm. However, the bulk of the prepared materials resembled the morphology exhibited by Cu-BDC prepared by El-Yazeed and Ahmed.[24] However, the metal oxide derived from Cu-BDC had no regular particle shape, which is evident in Figure 1. From the FESEM images, it could be seen that the prepared MOF had a higher surface area due to the rod-like surface morphology. The derived metal oxide, however, had a lower surface area because of the irregular surface particles. The analogy was well supported by the BET surface area analysis. The surface areas were found to be 715 m^2/g and 65 m^2/g for Cu-BDC and Cu-BDC derived metal oxides, respectively. EDX analysis of the prepared Cu-BDC was analyzed for carbon and oxygen species from the linker BDC and copper from the metal part. The EDX result confirmed the presence of carbon, oxygen, and copper in the prepared compound and provided the elemental composition ratio. Similarly for Cu_2O, the EDX analysis was carried out and the presence of carbon, copper, and oxygen was confirmed. The copper and oxygen were the elements from the Cu_2O

https://doi.org/10.1021/acsomega.2c03574
ACS Omega 2022, 7, 34966−34973

obtained after the oxidation of the Cu-BDC. The carbon species was formed from the conversion of the BDC in the nitrogen atmosphere.

XRD analysis of Cu-BDC is shown in Figure 2. The result obtained was monoclinic crystalline in nature. It was found

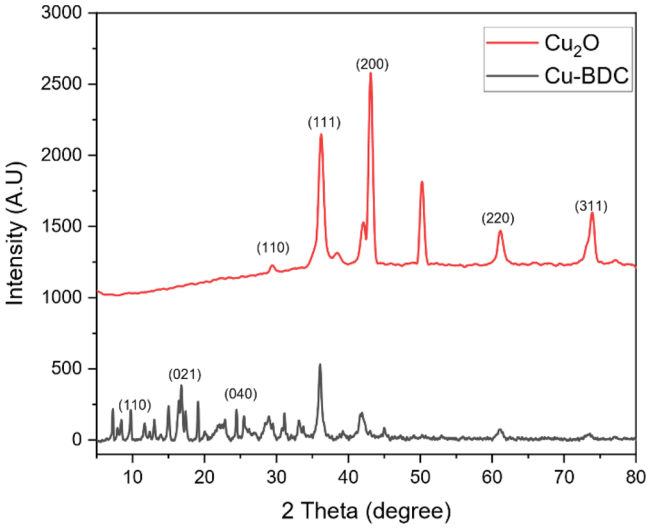

Figure 2. XRD of the prepared Cu_2O and Cu-BDC MOF.

that the average crystal size of Cu-BDC was 28 nm. The XRD spectra matched the Cambridge crystallographic information data with deposit number 112954, as observed by A. R. Bagheri and M. Ghaedi,[25] similar observations were made by Silva et al.[26] Similarly, the MOF derived metal oxide was characterized using XRD, and the XRD spectrum is shown in Figure 2. The XRD clearly shows the formation of Cu_2O. The peaks representing Cu_2O at 29°, 36°, 42°, 61°, and 73° were found in the XRD. The peaks were consistent with the standard JCPDS No. 05-0667.[27]

FTIR was carried out for both Cu-BDC and Cu_2O, and the spectrum was obtained in Figure 3. For the prepared Cu-BDC, the asymmetric and symmetric stretching of COO^- was seen at 1566 and 1367 cm^{-1}. The C═C and C−H of benzene from

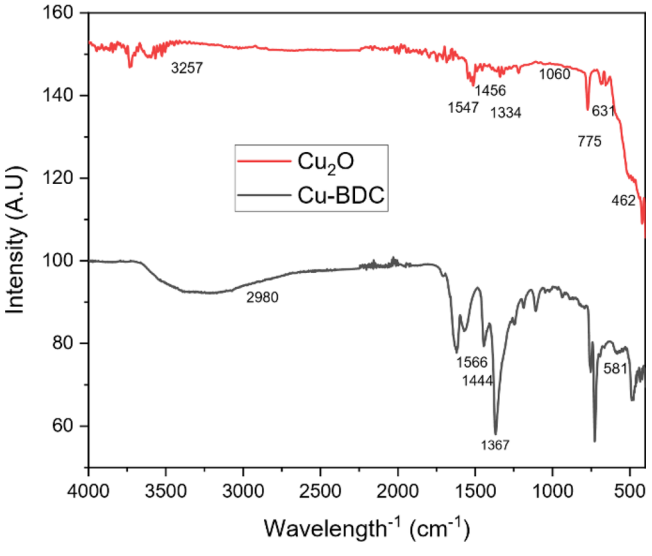

Figure 3. FTIR spectrum of prepared Cu_2O and Cu-BDC.

benzene dicarboxylic acid was observed at 1444 and 2980 cm^{-1}, respectively.[28] In addition to the BDC the Cu−O band at 581 cm^{-1} was found in the spectrum. In case of the MOF derived metal oxide, the characteristic Cu_2O peaks at 463 and 631 cm^{-1} were found, which determined that the prepared material was Cu_2O.[27]

Batch Adsorption Studies. The prepared Cu-BDC and Cu_2O were used in the studies of adsorption of asphaltenes by varying the dosage from 2.5 g/L to 25 g/L. The adsorption percentage of asphaltenes increased with the increase in the adsorbent dosage, and 0.5 g of Cu-BDC could adsorb 73.2% of the asphaltenes. Similarly in the case of Cu_2O, the maximum adsorption could be found using a 0.5 g Cu_2O dosage, with 94% removal.

The effect of the initial asphaltene concentration on the adsorption onto the adsorbates Cu-BDC and the Cu-BDC derived Cu_2O was studied by varying the initial concentration from 10 mg/L to 150 mg/L. It was observed that the percentage adsorption decreased with the increase of the initial concentration of asphaltenes in both cases. A maximum of 98% adsorption was observed for the adsorption of 10 mg/L of asphaltene concentration in the case of Cu-BDC. For the Cu-BDC derived Cu_2O, a maximum of 92% adsorption could be seen. With an increase in asphaltene concentration, the adsorption decreases due to a decrease in the active pore sites, that is, with the adsorption of asphaltenes, the surface area for the adsorption reduces due to the unavailability of pores in both Cu-BDC and Cu_2O.

These data were used to study the Langmuir and Freundlich adsorption isotherm models. The plots for the Langmuir and Freundlich isotherm models for Cu-BDC are shown in Figure 4. It could be observed that the predicted curve for the Langmuir isotherm was closer to the experimental data points when compared to the Freundlich isotherm model curve. Also, from Table 1, the value of r^2 was found to be 0.992 for the Langmuir isotherm, suggesting that the error was minimal for the Langmuir model when compared with the Freundlich model with respect to the experimental values, thereby rendering it the best fit model. Hence, the binding of asphaltene onto the prepared copper metal organic frameworks surface was by monolayer adsorption. The Langmuir and Freundlich isotherm parameters for the adsorption of asphaltene on the Cu-BDC are shown in Table 1. In the case of Cu_2O, as shown in Figure 4, the isotherm studies followed the Langmuir isotherm with an $r^2$of 0.975 and having a maximum adsorption capacity of 28 mg asphaltenes/g adsorbent. MOF derived metal oxide proved to be inferior to the adsorption performance of the MOF itself. The Cu-BDC had a 4-fold (123 mg asphaltenes/g adsorbent) higher adsorption capacity when compared with the Cu_2O derived from it. The variation in the adsorption could be due to the surface area of the MOF. In both cases, the Langmuir isotherm was found to be the governing model, suggesting monolayer adsorption. The Langmuir monolayer adsorption capacity of the prepared adsorbent for the adsorption of asphaltenes was compared with other adsorbents reported in the literature. It was inferred from Table 2 that Cu-BDC prepared in the current study had superior capacity compared to the reported adsorbents.

The time dependence of the uptake of asphaltenes using Cu-BDC and Cu_2O was studied by performing kinetic experiments. The kinetic data were interpreted with the most commonly used kinetic models, namely pseudo first order

https://doi.org/10.1021/acsomega.2c03574
ACS Omega 2022, 7, 34966−34973

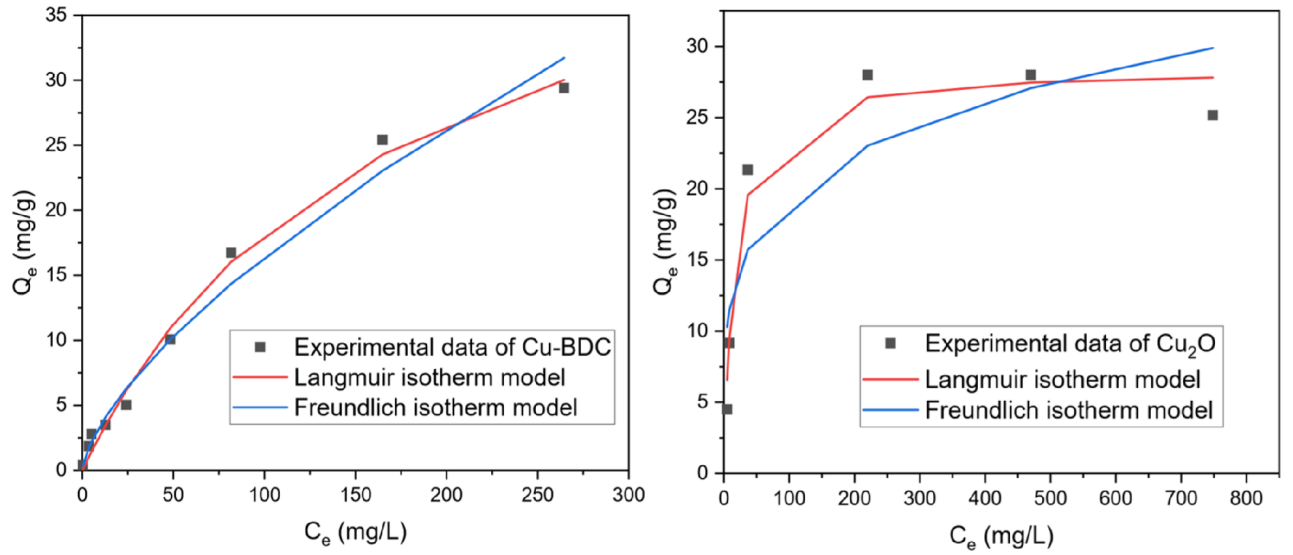

Figure 4. Langmuir and Freundlich isotherm model plots for the adsorption of asphaltenes using Cu-BDC and Cu_2O.

Table 1. Langmuir and Freundlich Isotherm Model Parameters for Adsorption of Asphaltenes Using Cu-BDC

adsorption isotherm	Langmuir isotherm model			Freundlich isotherm model		
	K_L (L/mg)	Q_0 (mg/g)	r^2	K_f (mg/g)	n	r^2
Cu-BDC	0.005	123.10	0.992	2.30	1.58	0.979
Cu_2O	0.06	28.43	0.975	7.30	4.69	0.829

Table 2. Adsorption Capacity of Cu-BDC and Cu_2O Compared with Reported Adsorbents for the Adsorption of Asphaltenes

adsorbent	maximum monolayer adsorption capacity(mg/g)	reference
NiO	60.1	29
Co_3O_4	63.1	
Fe_3O_4	62	
alumina	290	30
kaolinite	33.9	31
quartz	6.4	
γ-Al_2O_3	88.5	32
Fe_3O_4	73.1	33
TiO_2	98.1	
NiO	85.6	
CaO	79.6	
polythiophene coated Fe_3O_4	83.7	34
carbon nano tubes	384	35
NiO	420	36
Cu-BDC	123.1	current work
Cu_2O	28.43	

adsorption kinetics and pseudo second order adsorption kinetics models. The mechanism of adsorption of asphaltenes onto MOFs and metal oxides was studied by interpreting the kinetic data with the intraparticle diffusion model and Boyd plot.

Adsorption kinetics experiments were carried out for the adsorption of asphaltenes onto Cu-BDC and kinetic models were used to study the kinetics of the adsorption as shown in Figure S1 of the Supporting Information. The adsorbent dosage was fixed at 4 g/L. The kinetic data was tested with pseudo first order and pseudo second order kinetic models. It was found that the pseudo second order kinetic model was the best fit for Cu-BDC. The fitting of pseudo second order kinetics essentially means that the adsorption follows chemisorption. Due to the fact that the asphaltenes are a highly polar class of compounds, the possibility of chemisorption could be expected. Further, the equilibrium time adsorption process rightly points toward the possibility of chemisorption. In addition to the above observations, from Table 3, the predicted Q_e estimated from the pseudo second order kinetics was found to closely match the observed Q_e from experimentation. Similarly for Cu-BDC derived Cu_2O, the prepared Cu_2O was subjected to a kinetics study similar to that for Cu-BDC. From Figure S2, the Cu_2O adsorption reaction was found to follow the pseudo second order adsorption kinetics similar to Cu-BDC, suggesting a similar phenomenon in the adsorption process. The equilibrium time, however, was comparatively late, suggesting slower adsorption possibly due to lower surface interaction when compared to Cu-BDC.

The intraparticle diffusion model is used to determine the adsorption process of the adsorbate onto the adsorbent. The model describes the transport of the adsorbate toward the adsorbent and into the pores of the adsorbent. Typically, the intraparticle diffusion plot is divided into three stages: boundary layer diffusion, intraparticle diffusion, and final

Table 3. Model Parameters of Pseudo First Order (PFO) and Pseudo Second Order (PSO) Kinetics for Cu-BDC and Cu_2O

kinetic model	PFO adsorption model			PSO adsorption model			experimental
	Q_e (mg/g)	K_1 (h^{-1})	r^2	Q_e (mg/g)	K_2 (h^{-1})	r^2	Q_e (mg/g)
Cu-BDC	24.746	0.003	0.180	12.351	3.077	0.999	12.24
Cu_2O	10.354	0.006	0.274	33.014	0.331	0.999	33.4

https://doi.org/10.1021/acsomega.2c03574
ACS Omega 2022, 7, 34966−34973

equilibrium. In the case of multilinear curves in the Q_t vs $\sqrt{t}$ plot, more than one step influences the adsorption process. From Figure S3, the adsorption of asphaltenes onto Cu-BDC and Cu_2O traces a multilinear path, suggesting more than one step influencing the adsorption process. The curve could be divided into three regions with the origin as the starting point. The initial part of the adsorption process was driven by film diffusion, followed by intraparticle diffusion, and finally equilibrium adsorption. From Figure S3, the adsorption of asphaltenes over Cu-BDC was driven by film diffusion for about 2.5 min, and the intraparticle diffusion governed the reaction for about a minute to finally attain the equilibrium state. Whereas for asphaltenes adsorption onto Cu_2O, the film diffusion could be observed for about half an hour, followed by intraparticle diffusion driven adsorption for about an hour. The adsorption then attained a final equilibrium adsorption state after 2 h, which occurs after the asphaltenes are slowly driven into the pores of the nanocomposites. To further explain the rate limiting step of the asphaltenes adsorption process, the Boyd's diffusion kinetics model was applied. The Boyd's diffusion plot was plotted with B_t vs t as in Figure 5. The plots

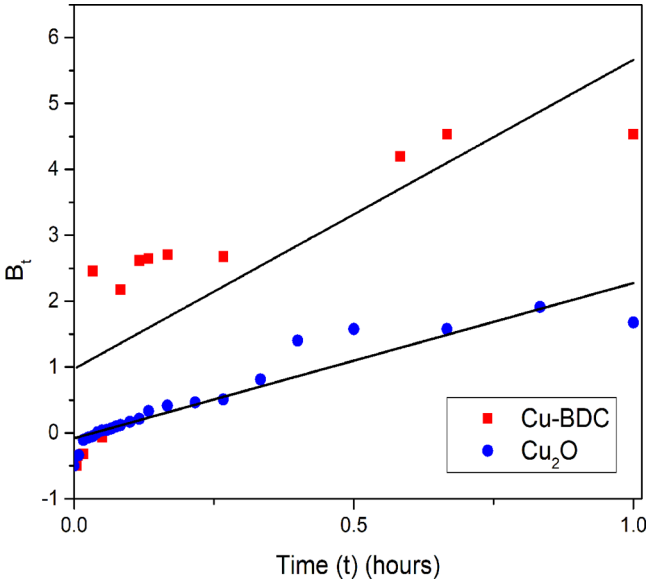

Figure 5. Boyd plot of the asphaltenes adsorption onto Cu_2O and Cu-BDC.

trace a straight line without passing through the origin or non-linear plots, the governing factor would be external mass transfer or film diffusion. The trend in the Boyd's plot for the asphaltenes adsorbed onto Cu-BDC and Cu_2O traces a straight line trend avoiding the origin, suggesting that the adsorption process was governed by film diffusion or external mass transfer.[37]

The asphaltenes adsorbed onto the nanocomposites were desorbed using xylene as solvent and about 45% desorption could be achieved. The studies were further carried out for 3 cycles and a desorption of 45−43% could be achieved in each cycle. The lower desorption could be because of the highly polar nature of the asphaltenes and chemisorption of the asphaltenes onto the nanocomposites, as suggested by the adsorption isotherm studies.

Oxidation Studies of Asphaltenes Adsorbed onto Nanocomposites. Oxidation studies of asphaltenes on the adsorbent were carried out to evaluate the performance of the adsorbent in oxidation reaction, which helps in the regeneration of the adsorbent. The regenerated adsorbents are then reused in the adsorption studies. Thermogravimetric analysis (TGA) was performed to evaluate the oxidation potential of Cu-BDC. The asphaltenes on the Cu-BDC were prepared with 50% weight loading of the asphaltenes. The TGA was carried out in air atmosphere with the temperature ranging from 50 °C to 700 °C. The results obtained from TGA are depicted in Figure 6 for Cu-BDC assisted oxidation of

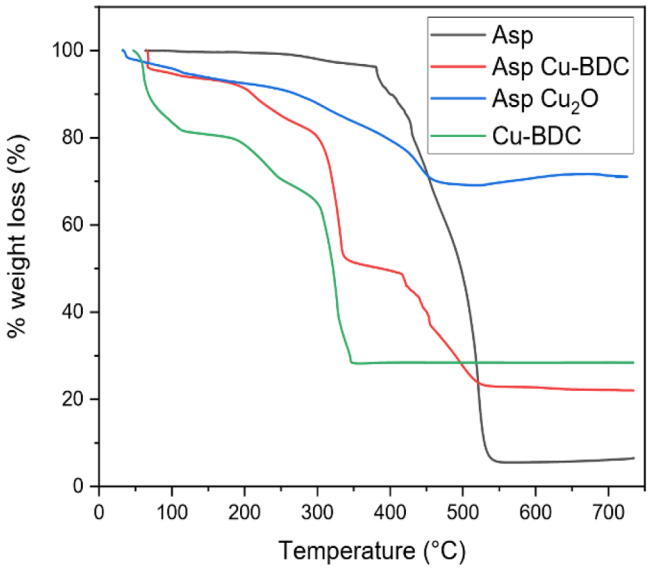

Figure 6. TGA of asphaltenes oxidation against Cu-BDC and Cu_2O assisted oxidation of asphaltenes along with Cu-BDC thermal degradation profile.

asphaltenes. The asphaltenes under study generally had an oxidation temperature of 530 °C. Although Cu-BDC was found to adsorb the asphaltenes to a significant extent, there was no improvement in the oxidation temperature of the asphaltenes. In fact, Cu-BDC could not maintain its original MOF form beyond 350 °C before it failed to catalyze the oxidation reaction of the asphaltenes. From Figure 6 it was evident that Cu-BDC decomposed at 350 °C and the oxidation of asphaltenes was unaltered with complete oxidation taking place at 530 °C. The residual weight in the Cu-BDC assisted oxidation thermograph represented the copper oxide that forms during Cu-BDC oxidation. Alternatively, the oxidation studies of asphaltenes on Cu_2O were carried out in the presence of air over the temperature range of 50 °C to 700 °C. The oxidation studies were carried out for 10 wt % asphaltenes loaded onto Cu_2O. The weight loss profile was obtained as in Figure 6. Cu_2O oxidized the asphaltenes with complete oxidation of the asphaltenes observed at 480 °C. The profile traces a flat line beyond 480 °C, indicating the stability of the prepared metal oxide at higher temperature. The asphaltenes oxidation catalyzed by Cu_2O was observed to reduce the oxidation temperature by 50 °C, suggesting that Cu_2O is participating in the oxidation reaction, unlike Cu-BDC. The improved stability along with the improved thermal tolerance of the metal oxide outperforms the oxidation catalyzed by the MOF. Hence, Cu_2O is superior to Cu-BDC in the oxidation of the asphaltenes.

https://doi.org/10.1021/acsomega.2c03574
ACS Omega 2022, 7, 34966−34973

EXPERIMENTAL SECTION

Materials. Copper nitrate trihydrate ($Cu(NO_3)_2.3H_2O$, Emplura, Merck India), *n*-Heptane (C_7H_{16}, 99%, LOBA Chemie India), terephthalic acid ($C_8H_6O_4$, 98%, Sigma-Aldrich U.S.A., BDC), dimethylformamide ($HCON(CH_3)_2$, extrapure, Finar India, DMF), and ethanol (C_2H_5OH, absolute, Hayman U.K.) were all used without further purification.

Extraction of Asphaltenes from Bitumen. Asphaltene extraction was carried out from heavy fraction using *n*-heptane in a ratio of 1:40 (1-part bitumen: 40 parts *n*-Heptane, ASTM D2007-80).[10] The mixture of bitumen and *n*-heptane was stirred for 24 h at room temperature and sonicated for an hour. The asphaltenes were filtrated on Whatman filter paper and separated from the solution. The wet asphaltenes were then dried in the hot air oven for 24 h. Furthermore, the asphaltenes model solution was prepared using 1 g asphaltenes in 1 L of toluene.

Preparation and Characterization of Nanocomposites. *Preparation of Cu-BDC.* Cu-BDC was synthesized using a solvothermal process.[25] 1 g of BDC was dissolved in DMF and ethanol (2:1) solvent. 4 g of Copper nitrate was added to the resulting solution and was completely dissolved to form a homogeneous solution. The resulting solution was charged to a Teflon-lined autoclave and maintained at 120 °C for 12 h. The end product was separated and washed with DMF and distilled water to obtain Cu-BDC. The Cu-BDC was then dried at 80 °C and used in further studies.

Preparation of Cu-BDC Based Metal Oxide. The prepared MOFs after washing and drying were used in the preparation of the MOF based metal oxides. The Cu-BDC was dried in hot air oven and charged to a split tube furnace for oxidation under nitrogen atmosphere. The MOF was oxidized at 650 °C for 3 h, and the resulting nanomaterial was then further characterized using XRD and FESEM.

Characterization of Prepared Nanocomposites. The prepared MOF, CU-BDC was characterized for various properties using BET surface area analysis, XRD, FE-SEM, and EDX. The surface area analysis was analyzed in Smart sorb 92/93 instrument using BET adsorption model. XRD of the prepared materials was carried out in a Rigaku Miniflex 600 (5^{th} gen). The X-ray generation was established by 40 kV and a current of 15 mA. X-ray generation was performed in the presence of a nickel filter and the scanning was done from 5−80°. The FE-SEM and EDX analysis was carried out in a Carl Zeiss ULTRA 55 instrument.

Adsorption and Desorption Studies of the Asphaltenes onto the Prepared Nanocomposites. The batch adsorption studies were conducted with an asphaltenes model solution with Cu-BDC and Cu-BDC derived metal oxide as the adsorbent. The batch adsorption studies included the effect of adsorbent dosage, the effect of initial asphaltenes concentration, and kinetic studies. The desorption studies of the asphaltenes adsorbed onto the nanocomposites were carried out using xylene as the solvent for 3 cycles.

Batch Adsorption Studies. The effect of adsorbent dosage studies included the variation of nanocomposite dosage from 0 g/L to 25 g/L, a 225 mg/L asphaltenes model solution was used in the studies and the studies were carried out at 32 °C, 200 rpm, and 24 h reaction time. The batch adsorption studies data were used to study the Langmuir and Freundlich adsorption isotherm models. The Langmuir model equation:[38]

$$Q_e = (Q_0 K_L C_e)/(1 + K_L C_e) \quad (1)$$

where C_e is the concentration of the adsorbate at equilibrium (mg/g), K_L is the equilibrium constant (L/mg), Q_e is the equilibrium adsorption capacity, and Q_0 is the maximum monolayer adsorption capacity.

The Freundlich model equation:[39]

$$Q_e = K_f C_e^{(1/n)} \quad (2)$$

where Q_e is the equilibrium adsorption capacity (mg/g), C_e is the concentration of the adsorbate at equilibrium (mg/g), and K_f is the adsorption coefficient and represents the adhesion ability of the adsorbate onto the adsorbent.

Effect of Initial Asphaltenes Concentration. The effect of initial asphaltenes concentration was carried out at 20 mL asphaltenes solution with 25 g/L adsorbents maintained at 32 °C, 200 rpm for 24 h reaction time. The initial asphaltenes concentration was varied from 10 to 150 mg/L.

Adsorption Kinetic Studies. The adsorption kinetics studies were carried out at 32 °C, 200 rpm for a time of 24 h. The adsorbent dosage was fixed to 1 g/L nanocomposite with the initial concentration of the asphaltenes solution fixed to 400 mg/L. The kinetic data was interpreted using pseudo first order and pseudo second order kinetic equation. The linear form of pseudo first order kinetic equation:[40]

$$\ln(Q_e - Q_t) = \ln(Q_e) - k_1 t \quad (3)$$

The linear form of pseudo second order kinetic equation:[41]

$$Q_t = t/(1/k_2 Q_e^2 + t/Q_e) \quad (4)$$

where Q_e is equilibrium adsorption capacity (mg/g), Q_t is the adsorption capacity at time "t" (mg/g), and k_1 and k_2 are rate constants.

The mechanism of the adsorption of asphaltenes onto MOFs and metal oxides was studied by interpreting the kinetic data with intraparticle diffusion model and Boyd plot.

The intraparticle diffusion model equation:[42]

$$Q_t = k_i \sqrt{t} + C \quad (5)$$

where Q_t is the adsorption capacity at time "t" (mg/g), and k_i is intraparticle diffusion rate constant (mg/g $min^{0.5}$).

The Boyd equation:[43]

$$B_t = -0.4977 - \ln(1 - F) \quad (6)$$

where F (dimensionless) is the fractional adsorption capacity.

Residual Concentration Analysis. The residual concentration from each of the studies was estimated using a SHIMADZU/UV 1800 SERIES UV−Visible spectrophotometer. The estimation was carried out at 800 nm wavelength with toluene as reference. The adsorbent was separated from the residual asphaltenes solution using a centrifuge.

Oxidation Studies of the Asphaltenes over Prepared Nanocomposites. The prepared materials were further used in the oxidative degradation of asphaltenes using thermogravimetric analysis (TGA). The TGA analysis was carried out in a TA 55 Discovery instrument (TA Instruments, Austria) under air supply. The oxidation was carried over the range of 50 °C to 700 °C during which the weight loss and derivative weight loss were recorded.

https://doi.org/10.1021/acsomega.2c03574
ACS Omega 2022, 7, 34966−34973

CONCLUSIONS

Asphaltenes are regarded as the cholesterol of petroleum crude. An increased amount of asphaltenes production can be seen with heavier crude production. The petroleum and fossil industries pour in huge sums of money to maintain the equipment from asphaltenes fouling. The strategy of using nanotechnology to overcome this problem is fairly new and the MOFs for this application has not been explored. Reasons to avoid MOFs could include the thermal decomposition of MOFs at low temperatures. This makes MOF a one-time use material. In this work, Cu-BDC MOF and Cu_2O derived from Cu-BDC have been used for the removal and oxidation of asphaltenes. The comparative study of asphaltene adsorption on Cu-BDC and Cu_2O was found to be monolayer adsorption following the Langmuir isotherm. As seen in previous studies of MOFs in adsorption, Cu-BDC was found to have higher adsorption capacity (123 mg asphaltenes/g adsorbent), in comparison with Cu_2O (28 mg asphaltenes/g adsorbent). The adsorption kinetics studies on both adsorbents showed that the adsorption process was pseudo second order, and the intraparticle diffusion model showed that the process followed film diffusion at the start, followed by intraparticle diffusion, and ending with a final equilibrium stage. In addition, the Boyd plot suggested film diffusion as the rate limiting step. The oxidation studies of asphaltenes over the adsorbents were carried out in an air atmosphere. Cu-BDC naturally had no catalytic behavior because of the low decomposition temperature. However, unlike Cu-BDC, Cu-BDC derived Cu_2O reduced the oxidation temperature by 50 °C without decomposing. Therefore, the adsorption process was dominated by Cu-BDC, and the oxidation catalysis and thermal tolerance was superior in Cu_2O. In conclusion, the MOFs can be used for the adsorption of asphaltenes and can be reused in the form of metal oxides in the adsorption and oxidation of asphaltenes.

ASSOCIATED CONTENT

Supporting Information

The Supporting Information is available free of charge at https://pubs.acs.org/doi/10.1021/acsomega.2c03574.

Adsorption reaction kinetics of Cu-BDC and Cu_2O involving pseudo first order and pseudo second order model fitting and the intraparticle diffusion model fitting (PDF)

AUTHOR INFORMATION

Corresponding Author

Nethaji Sundarabal − *Department of Chemical Engineering, Manipal Institute of Technology, Manipal, Karnataka 576104, India;* orcid.org/0000-0002-7346-7838; Phone: 0820 2924316; Email: nethajis6587@gmail.com

Authors

Abhishek Nayak − *Department of Chemical Engineering, Manipal Institute of Technology, Manipal, Karnataka 576104, India*

Shanon Viegas − *Department of Chemical Engineering, Manipal Institute of Technology, Manipal, Karnataka 576104, India*

Harshini Dasari − *Department of Chemical Engineering, Manipal Institute of Technology, Manipal, Karnataka 576104, India;* orcid.org/0000-0001-9410-4369

Complete contact information is available at: https://pubs.acs.org/10.1021/acsomega.2c03574

Notes

The authors declare no competing financial interest.

ACKNOWLEDGMENTS

The authors would like to thank Manipal Academy of Higher Education, Karnataka for providing financial support and the facilities throughout this work.

REFERENCES

(1) Rashid, Z.; Wilfred, C. D.; Gnanasundaram, N.; Arunagiri, A.; Murugesan, T. A comprehensive review on the recent advances on the petroleum asphaltene aggregation. *J. Pet. Sci. Eng.* **2019**, *176*, 249−268.

(2) Luo, P.; Gu, Y. Effects of asphaltene content on the heavy oil viscosity at different temperatures. *Fuel* **2007**, *86*, 1069−1078.

(3) Shayan, N. N.; Mirzayi, B. Adsorption and removal of asphaltene using synthesized maghemite and hematite nanoparticles. *Energy Fuels* **2015**, *29*, 1397−1406.

(4) Gray, M. R. *The Chemistry and Technology of Petroleum*, 2nd ed., revised and expanded; Speight, J. G., Ed.; Marcel Dekker: New York, 1991; Vol. *38*, pp 1304−1305.

(5) Mack, C. Colloid chemistry of asphalts. *J. Phys. Chem.* **1932**, *36*, 2901−2914.

(6) Contreras-Mateus, M. D.; Sánchez, F. H.; Cañas-Martínez, D. M.; Nassar, N. N.; Chaves-Guerrero, A. Effect of asphaltene adsorption on the magnetic and magnetorheological properties of heavy crude oils and Fe3O4 nanoparticles systems. *Fuel* **2022**, *318*, 123684.

(7) Mazloom, M. S.; Hemmati-Sarapardeh, A.; Husein, M. M.; Behbahani, H. S.; Zendehboudi, S. Application of nanoparticles for asphaltenes adsorption and oxidation: A critical review of challenges and recent progress. *Fuel* **2020**, *279*, 117763.

(8) Shojaei, B.; Miri, R.; Bazyari, A.; Thompson, L. T. Asphaltene adsorption on MgO, CaO, SiO2, and Al2O3 nanoparticles synthesized via the Pechini-type Sol- Gel method. *Fuel* **2022**, *321*, 124136.

(9) Marczewski, A. W.; Szymula, M. Adsorption of asphaltenes from toluene on mineral surface. *Colloids Surf. A Physicochem. Eng. Asp.* **2002**, *208*, 259−266.

(10) Zhang, H.; Sun, S.; Wang, X.; Wu, D. Fabrication of microencapsulated phase change materials based on n-octadecane core and silica shell through interfacial polycondensation. *Colloids Surf. A Physicochem. Eng. Asp.* **2011**, *389*, 104−117.

(11) Dudášová, D.; Simon, S.; Hemmingsen, P. V.; Sjöblom, J. Study of asphaltenes adsorption onto different minerals and clays: Part 1. Experimental adsorption with UV depletion detection. *Colloids Surf. A Physicochem. Eng. Asp.* **2008**, *317*, 1−9.

(12) Girard, H.-L.; Bourrianne, P.; Chen, D.; Jaishankar, A.; Vreeland, J. L.; Cohen, R. E.; Varanasi, K. K.; McKinley, G. H. Asphaltene adsorption on functionalized solids. *Langmuir* **2020**, *36*, 3894−3902.

(13) Hosseini-Dastgerdi, Z.; Meshkat, S. S. An experimental and modeling study of asphaltene adsorption by carbon nanotubes from model oil solution. *J. Pet. Sci. Eng.* **2019**, *174*, 1053−1061.

(14) Jiang, D.; Chen, M.; Wang, H.; Zeng, G.; Huang, D.; Cheng, M.; Liu, Y.; Xue, W.; Wang, Z. The application of different typological and structural MOFs-based materials for the dyes adsorption. *Coord. Chem. Rev.* **2019**, *380*, 471−483.

(15) Valenzano, L.; Civalleri, B.; Chavan, S.; Palomino, G. T.; Areán, C. O.; Bordiga, S. Computational and Experimental Studies on the Adsorption of CO, N2, and CO2 on Mg-MOF-74. *J. Phys. Chem. C* **2010**, *114*, 11185−11191.

(16) Belmabkhout, Y.; Bhatt, P. M.; Adil, K.; Pillai, R. S.; Cadiau, A.; Shkurenko, A.; Maurin, G.; Liu, G.; Koros, W. J.; Eddaoudi, M.

Natural gas upgrading using a fluorinated MOF with tuned H2S and CO2 adsorption selectivity. *Nat. Energy* **2018**, *3*, 1059−1066.
(17) Chen, F.; Lai, D.; Guo, L.; Wang, J.; Zhang, P.; Wu, K.; Zhang, Z.; Yang, Q.; Yang, Y.; Chen, B.; et al. Deep Desulfurization with Record SO2 Adsorption on the Metal−Organic Frameworks. *J. Am. Chem. Soc.* **2021**, *143*, 9040−9047.
(18) Zhou, W.; Wu, H.; Yildirim, T. Enhanced H2 adsorption in isostructural metal- organic frameworks with open metal sites: strong dependence of the binding strength on metal ions. *J. Am. Chem. Soc.* **2008**, *130*, 15268−15269.
(19) Bao, Z.; Yu, L.; Ren, Q.; Lu, X.; Deng, S. Adsorption of CO2 and CH4 on a magnesium-based metal organic framework. *J. Colloid Interface Sci.* **2011**, *353*, 549−556.
(20) Adeyemo, A. A.; Adeoye, I. O.; Bello, O. S. Metal organic frameworks as adsorbents for dye adsorption: overview, prospects and future challenges. *Toxicol. Environ. Chem.* **2012**, *94*, 1846−1863.
(21) Wang, C.; Xiong, C.; He, Y.; Yang, C.; Li, X.; Zheng, J.; Wang, S. Facile preparation of magnetic Zr-MOF for adsorption of Pb (II) and Cr (VI) from water: Adsorption characteristics and mechanisms. *CMEJAJ.* **2021**, *415*, 128923.
(22) Valizadeh, B.; Nguyen, T. N.; Kampouri, S.; Sun, D. T.; Mensi, M. D.; Stylianou, K.; Smit, B.; Queen, W. L. A novel integrated Cr (VI) adsorption−photoreduction system using MOF@ polymer composite beads. *J. Mater. Chem. A* **2020**, *8* (9), 9629−9637.
(23) Healy, C.; Patil, K. M.; Wilson, B. H.; Hermanspahn, L.; Harvey-Reid, N. C.; Howard, B. I.; Kleinjan, C.; Kolien, J.; Payet, F.; Telfer, S. G.; et al. The thermal stability of metal-organic frameworks. *Coord. Chem. Rev.* **2020**, *419*, 213388.
(24) El-Yazeed, W. A.; Ahmed, A. I. Monometallic and bimetallic Cu−Ag MOF/MCM-41 composites: structural characterization and catalytic activity. *RSC Adv.* **2019**, *9*, 18803−18813.
(25) Bagheri, A. R.; Ghaedi, M. Application of Cu-based metal-organic framework (Cu-BDC) as a sorbent for dispersive solid-phase extraction of gallic acid from orange juice samples using HPLC-UV method. *Arabian J. Chem.* **2020**, *13*, 5218−5228.
(26) Silva, B. C.; Irikura, K.; Flor, J. B. S.; Dos Santos, R. M. M.; Lachgar, A.; Frem, R. C. G.; Zanoni, M. V. B. Electrochemical preparation of Cu/Cu2O-Cu (BDC) metal-organic framework electrodes for photoelectrocatalytic reduction of CO2. *J. CO2 Util.* **2020**, *42*, 101299.
(27) Gupta, D.; Meher, S.; Illyaskutty, N.; Alex, Z. C. Facile synthesis of Cu2O and CuO nanoparticles and study of their structural, optical and electronic properties. *J. Alloys Compd.* **2018**, *743*, 737−745.
(28) Abdelhamid, H. N. High performance and ultrafast reduction of 4-nitrophenol using metal-organic frameworks. *J. Environ. Chem. Eng.* **2021**, *9*, 104404.
(29) Nassar, N. N.; Hassan, A.; Pereira-Almao, P. Comparative oxidatizon of adsorbed asphaltenes onto transition metal oxide nanoparticles. *Colloids Surf. A Physicochem. Eng. Asp.* **2011**, *384*, 145−149.
(30) Guichard, B.; Gaulier, F.; Barbier, J.; Corre, T.; Bonneau, J.-L.; Levitz, P.; Espinat, D. Asphaltenes diffusion/adsorption through catalyst alumina supports−Influence on catalytic activity. *Catal. Today* **2018**, *305*, 49−57.
(31) Pernyeszi, T.; Patzkó, Á.; Berkesi, O.; Dékány, I. Asphaltene adsorption on clays and crude oil reservoir rocks. *Colloids Surf. A Physicochem. Eng. Asp.* **1998**, *137*, 373−384.
(32) Nassar, N. N. Asphaltene adsorption onto alumina nanoparticles: kinetics and thermodynamic studies. *Energy Fuels* **2010**, *24*, 4116−4122.
(33) Nassar, N. N.; Hassan, A.; Pereira-Almao, P. Metal oxide nanoparticles for asphaltene adsorption and oxidation. *Energy Fuels* **2011**, *25*, 1017−1023.
(34) Setoodeh, N.; Darvishi, P.; Esmaeilzadeh, F. Adsorption of asphaltene from crude oil by applying polythiophene coating on Fe3O4 nanoparticles. *J. Dispersion Sci. Technol.* **2018**, *39*, 578−588.
(35) Hosseini-Dastgerdi, Z.; Meshkat, S. S. An experimental and modeling study of asphaltene adsorption by carbon nanotubes from model oil solution. *J. Pet. Sci. Eng.* **2019**, *174*, 1053−1061.
(36) Tarboush, B. J. A.; Husein, M. M. Adsorption of asphaltenes from heavy oil onto in situ prepared NiO nanoparticles. *J. Colloid Interface Sci.* **2012**, *378*, 64−69.
(37) Rashidi, N. A.; Bokhari, A.; Yusup, S. Evaluation of kinetics and mechanism properties of CO2 adsorption onto the palm kernel shell activated carbon. *Environ. Sci. Pollut. Res.* **2021**, *28*, 33967−33979.
(38) Langmuir, I. The adsorption of gases on plane surfaces of glass, mica and platinum. *J. Am. Chem. Soc.* **1918**, *40*, 1361−1403.
(39) Freundlich, H. Over the adsorption in solution. *J. Phys. Chem.* **1906**, *57*, 1100−1107.
(40) Santhy, K.; Selvapathy, P. Removal of reactive dyes from wastewater by adsorption on coir pith activated carbon. *Bioresour. Technol.* **2006**, *97*, 1329−1336.
(41) Bulut, E.; Özacar, M.; Şengil, İ. A. Adsorption of malachite green onto bentonite: equilibrium and kinetic studies and process design. *Micropor Mesopor Mat* **2008**, *115*, 234−246.
(42) Cheung, W.; Szeto, Y.; McKay, G. Intraparticle diffusion processes during acid dye adsorption onto chitosan. *Bioresour. Technol.* **2007**, *98*, 2897−2904.
(43) Kumar, K. V.; Ramamurthi, V.; Sivanesan, S. Modeling the mechanism involved during the sorption of methylene blue onto fly ash. *J. Colloid Interface Sci.* **2005**, *284*, 14−21.

https://doi.org/10.1021/acsomega.2c03574
ACS Omega 2022, 7, 34966−34973